THE ASTROPHYSICAL JOURNAL, 451:359–371, 1995 September 20

ULTRAVIOLET TEMPORAL VARIABILITY OF THE PECULIAR STAR R AQUARII

STEVEN R. MEIER[1]
Space and Environment Technology Center, Remote Sensing Department, The Aerospace Corporation, Los Angeles, CA 90009

AND

MENAS KAFATOS[2]
Center for Earth Observing and Space Research/CSI Institute and Department of Physics, George Mason University, Fairfax, VA 22030-4444
Received 1994 September 12; accepted 1995 March 30

ABSTRACT

This paper is a comprehensive study of all far-UV spectra obtained with the *International Ultraviolet Explorer* (*IUE*) satellite of the symbiotic star R Aquarii (R Aqr) covering a 13 yr period between 1979 and 1992. We have analyzed the ultraviolet emission for the compact H II region and the NE and SW extended "jetlike" filamentary structures. The results of our ultraviolet analysis indicate that the H II region and features A, B, and D of the NE jet are increasing in intensity, while the SW counterjet, feature A′, has declined in intensity. We have found much stronger evidence that the high ionization lines of N V $\lambda\lambda$1238, 1240 and He II λ1640 in the H II region and NE jet have steadily increased over the entire period of *IUE* observations. This result could indicate that the ionized region is increasing in excitation. We have found that the observations of the NE jet are consistent with a decreasing electron temperature and increasing line-emitting region, which suggest that the strengthening of emission-line fluxes may be a result of an expanding emitting volume in a post-shocked region. Low-resolution absolute line intensities and wavelengths for the most prominent emission lines in the $\lambda\lambda$1200–3200 wavelength range have been tabulated. In addition, we present plots of the total ultraviolet flux ($\lambda\lambda$1200–3200) and absolute line intensities as a function of time to discern the temporal variability of R Aqr. These plots indicate that the far-UV emission from the NE jet is not variable on a $\sim$1.5 yr timescale as suggested by Kafatos, Michalitsianos, & Hollis. Moreover, we find that the variations in the far-UV emission in R Aqr are not coupled to the 386 day pulsation period of the Mira. Finally, successive ionization levels of carbon, nitrogen, oxygen, and silicon of the NE jet are compared with each other to probe the nature of the ionization source in the NE jet.

High- and low-resolution ultraviolet spectra were used to calculate the properties of the emission nebula and hot component. We determined electron densities of $n_e = 4 \times 10^5$ cm^{-3} (H II region) and $n_e = 6 \times 10^4$ cm^{-3} (NE jet), electron temperatures of $T_e \sim 20{,}000$ K (H II region) and a high value of $T_e \geq 26{,}000$ K between 1982 May and 1983 December, to a low value of $T_e \leq 18{,}000$ K from observations during the period of 1986 December and 1989 June (NE jet), and also line-emitting regions of $L = 6.3 \times 10^{14}$ cm (H II region) and $L = 1.5 \times 10^{15}$ cm (NE jet). The He II λ1640 modified Zanstra method yielded an effective temperature of $T_* = 61{,}000$ K for the hot component. Estimates of the number of ionizing photons beyond the Lyman limit, blackbody parameters, and possible accretion disk parameters for the hot component are also given.

Subject headings: binaries: symbiotic — H II regions — ISM: jets and outflows — stars: individual (R Aquarii) — stars: peculiar — ultraviolet: stars

1. INTRODUCTION

This work is concerned with studying the far-ultraviolet temporal variations and physical parameters of the symbiotic star R Aquarii. A previous paper by Kafatos, Michalitsianos, & Hollis (1986) studied the far-UV variability over a 4 yr period from 1982 May to 1985 August. However, as a result of a much smaller data set, the results were limited in scope. In order to add more insight to this intriguing system, we believe an analysis of all existing ultraviolet data obtained with the *IUE* satellite may help to determine how far-UV emission and nebular parameters vary with time. This analysis could provide clues to the emission mechanisms in R Aqr, and since R Aqr is the nearest star which shows jet activity, to astrophysical jets in general.

Since the discovery of a complex jet structure, the peculiar symbiotic star R Aquarii (R Aqr) has been the subject of many inquiries. This binary star system contains a recently formed jet (Wallerstein & Greenstein 1980) and possibly an associated accretion disk (Kafatos et al. 1986). At a distance of $\sim$250 pc (Whitelock 1987), R Aqr is the closest symbiotic star as well as astrophysical jet, and with a 44 yr period (Willson, Garnavich, & Mattei 1981), it has the longest known binary orbit of any symbiotic. This complex system has been detected at virtually every wavelength from radio to soft X-rays. In addition to a wide range of excitation, R Aqr is the only known symbiotic system associated with SiO maser emission (Lepine, Le Squeren, & Scalise 1978).

R Aqr (M7e + pec) is believed to consist of a hot subdwarf or white dwarf and a Mira variable that is embedded in a compact H II region. The 386 day Mira has an ephemeris of max (V) = JD 2382892 + 386.3*E (Mattei & Allen 1979). This system has been known to undergo erratic outbursts. The most

[1] Present address: University of California at San Diego, Department of Electrical Engineering, Mail Code 0407, La Jolla, CA 92093-0407.
[2] *IUE* Guest Observer.

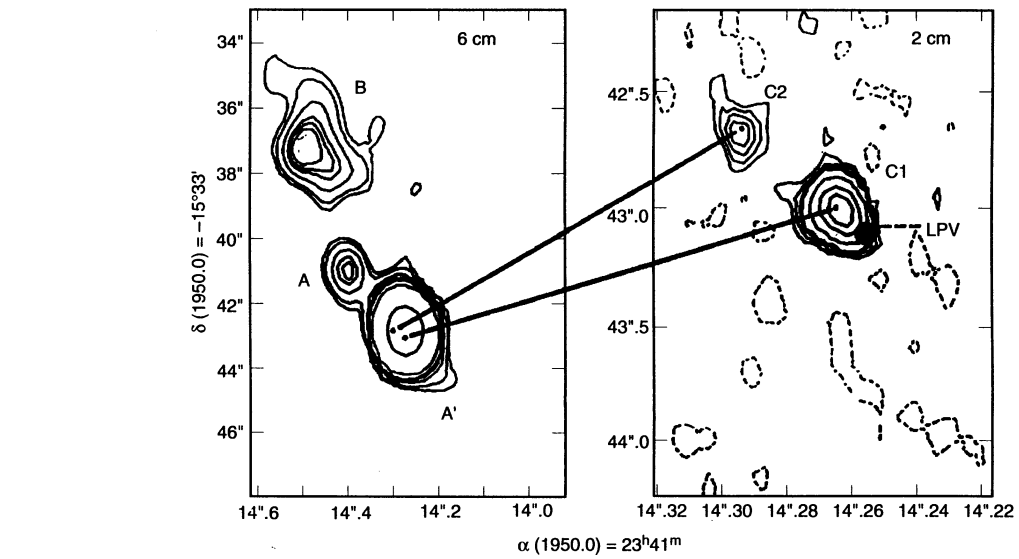

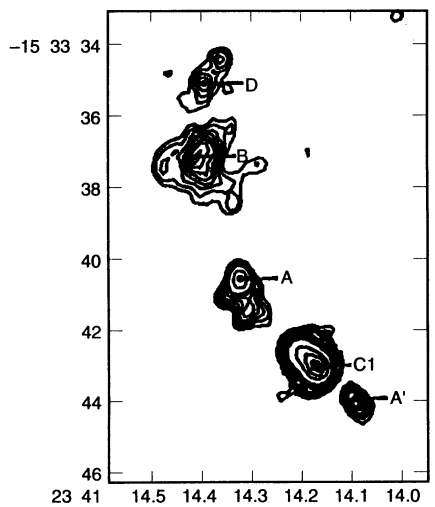

FIG. 1.—(*Bottom*) VLA 6 cm observations of configurations A, B, D, C1, and A′ of R Aquarii. (*Top*) VLA 2 cm and 6 cm maps of R Aquarii obtained by Hollis et al. (1985) of C1 (H II region), C2, A, and B (NE jet), and A′ (SW jet). Relative to feature C1, feature C2 is 0.″5 at P.A. = 55°, feature A is 2.″5 at P.A. = 45°, and feature B is 6.″5 at P.A. = 29°. Also shown is the 386 day LPV (Mira variable).

recently recorded outburst occurred between 1928 and 1935 in which the hot companion achieved a visual magnitude m_V of ~ 8, rivaling the visual light of the Mira (Mattei & Allen 1979).

The existence of extended jet structure is one of the features that makes R Aqr a unique astronomical object. In 1977, Wallerstein & Greenstein (1980) detected a "jet" of nebular material in the optical spectral region extending $\sim 6''$ NE of R Aqr Herbig (1980) confirmed the existence of the jet from optical plates taken in 1980. Observations by Sopka et al. (1982) first detected the NE jet in the radio region with the VLA.[3] Further VLA radio frequency observations by Kafatos, Hollis, & Michalitsianos (1983) at 6 cm resolved the system into three discrete regions of emission: (1) feature B at 6.″5 from R Aqr at a position angle of 29°, (2) feature A at 2.″5 and 45°, both related to the NE jet, and (3) the compact H II region (Fig. 1). Hollis et al. (1986), using 2 cm VLA observations, found the presence of two distinct emitting regions, C1 (the H II region) and C2. Recent *Hubble Space Telescope* (*HST*) observations obtained with the Faint Object Camera (FOC) centered at $\lambda = 1230$ Å determined that feature C1 itself consists of four distinct components (Burgarella & Paresce 1992; Paresce & Hack 1994). From near-UV observations, Mauron et al. (1985) discovered a counter jet (feature A′) in the SW direction. Additional observations at 6 cm by Kafatos et al. (1989) detected radio continuum emission in the counterjet, which extends approximately 10″ SW of R Aqr at a position angle of 231°. The most recently discovered emission feature, feature D, was found at $\sim 8.''4$ from the central object C1 with a position angle of 20° (Paresec, Burrows, & Horne 1988) (see Fig. 1).

The position of the *IUE* 10″ × 20″ aperture relative to the R Aqr radio morphology can be found in Michalitsianos & Kafatos (1988). The large size of the *IUE* aperture allows integrated ultraviolet emission in the H II region nebulosity primarily from features C1, C2, A, and A′, whereas the placing of the aperture in the NE jet integrates UV emission primarily from features A, B, and D.

Ultraviolet observations of R Aqr exhibit several emission lines of O I λλ1302–1306, C II λλ1334, 1335, C IV λλ1548, 1550, O III] λλ1660, 1666, N III] λλ1747–1753, Si III] λ1892, C III] λλ1907, 1909, C II] λλ2325, 2326, [O II] λ2470, and Mg II λλ2975, 2803. These emission lines are superposed on a UV continuum which gradually rises with decreasing wavelength in the NE jet (Michalitsianos & Kafatos 1982) and is essentially independent of wavelength for the central star and associated nebulosities (Johnson 1980, 1982; Michalitsianos, Kafatos, & Hobbs 1980; Meier et al. 1994). However, UV spectra of the H II region taken between 1986 October and 1991 December reveal a continuum flux that increases toward shorter wavelengths, similar to the NE jet. The appearance of N V λλ1238, 1240 and He II λ1640 emission in the NE and SW jets, compared with the weakness of N V and He II in the H II region, gives evidence that higher excitation conditions are present in the two jet structures (Michalitsianos, Hollis, & Kafatos 1986; Kafatos et al. 1986; Hollis et al. 1991). The

[3] The VLA of the National Radio Astronomy Observatory is operated by Associated Universities Inc., under contract with the NSF.

presence of N v emission in the NE jet is also consistent with the detection of soft X-ray emission in the 0.25–1 KeV range observed by the *EXOSAT* satellite (Viotti et al. 1987).

2. ULTRAVIOLET OBSERVATIONS

All *IUE* spectra of R Aquarii were obtained from the data archive of the *IUE* Regional Data Analysis Facility (RDAF) at NASA Goddard Space Flight Center (NASA/GSFC). In all, 82 *IUE* ultraviolet spectra in both the short-wavelength prime (SWP) and long-wavelength prime/long-wavelength redundant (LWP/LWR) regions ($\lambda\lambda$1200–3200) of the symbiotic star R Aquarii were retrieved and analyzed. The *IUE* spectra examined include 45 SWP ($\lambda\lambda$1200–2000) low-resolution, 29 LWP/LWR ($\lambda\lambda$2000–3200) low-resolution, five SWP high-resolution, and three LWP/LWR high-resolution spectra of the H II region, NE and SW jets. The ultraviolet spectra were obtained with the 10″ × 20″ large-aperture *IUE* spectrometer, which has a limiting spectral resolution of $\Delta\lambda \sim 6$ Å for low-dispersion spectra and $\Delta\lambda \sim 0.1$ Å for high-dispersion spectra. The *IUE* ultraviolet spectra presented have been analyzed using IDL (Interactive Design Language) data reduction routines developed at the RDAF at NASA/GSFC. Since the *IUE* spectra were collected at different epochs, all spectra have been reprocessed using the most current *IUE* Spectral Image Processing System (IUESIPS) data reduction routines. This ensures that all UV data have been analyzed using the same photometric calibration and extraction procedures.

The absolute emission-line intensity is affected by the calibration errors and the signal-to-noise ratio. These errors can lead to *IUE* uncertainties in the observed emission line flux of ~4%–5% for the strongest lines and ~10%–15% for moderately exposed lines. It should also be noted that the UV spectra have not been corrected for extinction because the absorption in R Aqr appears to be largely circumstellar and may even be time-dependent (Brugel et al. 1984).

Low-resolution UV spectra of the H II region, NE jets, and SW jets are presented in Figures 1*a*–1*h*, 2*a*–2*f*, and 3*a*–3*b*, respectively. Table 1 contains the observational parameters for all low-resolution SWP, LWP, and LWR spectra shown in these figures. The *IUE* spectra presented here represent a partial list of the total UV spectra that were analyzed. The images presented have good signal-to-noise ratios and were neither underexposed or saturated. Table 2 gives the low-resolution absolute line intensities and wavelengths for the most prominent emission lines in SWP (1200–2000 Å) and LWP/LWR (2000–3200 Å) wavelength ranges for the H II region, NW jets, and SW jets, respectively.

3. DATA ANALYSIS

The results of UV observations and analysis are described in this section along with the associated nebular, stellar, and possible accretion disk parameters.

3.1. *UV Lines and Continuum*

As shown in Figures 2*a*–2*d*, 3*a*–3*d*, and 4*a*–4*b*, the H II, NE jet, and SW jet region UV spectra of R Aqr are dominated by many resonance, semiforbidden, and forbidden emission lines. The ionization potentials found in R Aqr span a broad range from N V $\lambda\lambda$1238, 1242 (IP = 97.9 eV) to O I $\lambda\lambda$1302–1306 (IP = 13.6 eV). The strongest line in both regions (C III] $\lambda\lambda$1907, 1909) is overexposed in all spectra as a result of the dynamic range limitations, of order ~10, of the *IUE* SEC Vidicon detectors.

The first spectrum (Fig. 2*a*) of the H II region taken in 1980 November shows emission lines of C IV, C III], C II] + [O III], [O II], and Mg II superposed in a flat, moderately strong continuum. The UV continuum did not change noticeably in Figure 2*b* (1983 May) and line intensities remained constant, except for C III] and Mg II, which increased by ~1.5 times. In Figure 2*c* (1986 October), the absolute continuum increased

TABLE 1

LIST OF *IUE* OBSERVATIONS

Camera/Image Sequence Number	Julian Date	Date	Dispersion	Exposure (minutes)	Region
LWR 4619	2,444,022	1979 May 28	High	60	H II
SWP 10557	2,444,552	1980 Nov 8	Low	100	H II
SWP 10558	2,444,552	1980 Nov 8	High	240	H II
LWR 9251	2,444,552	1980 Nov 8	Low	60	H II
LWR 9255	2,444,553	1980 Nov 9	High	240	H II
SWP 20068	2,445,480	1983 May 25	Low	240	NE Jet
LWR 16013.....	2,445,480	1983 May 25	Low	20	H II
SWP 20069	2,445,480	1983 May 25	Low	40	H II
LWR 16016.....	2,445,481	1983 May 26	Low	90	NE Jet
SWP 29542	2,446,729	1986 Oct 25	Low	45	H II
LWP 9402	2,446,729	1986 Oct 25	Low	45	H II
SWP 29543	2,446,731	1986 Oct 27	High	765	NE Jet
SWP 29989	2,446,794	1986 Dec 29	Low	240	NE Jet
LWP 9814	2,446,794	1986 Dec 29	Low	120	NE Jet
SWP 31102	2,446,951	1987 Jun 4	High	770	H II
SWP 32645	2,447,161	1987 Dec 31	Low	240	NE Jet
LWP 12404.....	2,447,161	1987 Dec 31	Low	100	NE Jet
SWP 36397	2,447,683	1989 Jun 5	Low	200	NE Jet
LWP 15662.....	2,447,683	1989 Jun 5	Low	100	NE Jet
SWP 37914	2,447,889	1989 Dec 28	Low	300	SW Jet
SWP 40265	2,448,229	1990 Dec 3	High	115	H II
SWP 41699	2,448,403	1991 May 26	Low	50	H II
LWP 20449.....	2,448,403	1991 May 26	Low	40	H II
SWP 41706	2,448,404	1991 May 27	Low	260	SW Jet
LWP 21998.....	2,448,604	1991 Dec 13	High	345	H II
SWP 46585	2,448,983	1992 Dec 26	High	395	H II

TABLE 2A

LOW-RESOLUTION H II REGION ULTRAVIOLET SPECTRA OF R AQUARII

ION	λ(lab) (Å)	λ(IUE)[a] (Å)	FLUX[b] SWP 10557, LWR 9251	SWP 20069, LWR 16013	SWP 29542, LWP 9402	SWP 41699, LWP 20449
N V	1238.8, 1242.8	1242.7	...	...	1.8	1.8
O I	1301.1, 1304.9, 1306.0	1305.9	2.1	1.4	1.3	2.4
C II	1334.5, 1335.7	1335.7	1.3	1.1	1.8	2.6
Si IV	1393.8	1394.2	0.9	0.8	1.5	2.5
O IV]	1397.2, 1399.8, 1401.1	1403.1	1.3	1.2	1.9	2.7
	1404.8, 1407.3	...	...	...	...	...
N IV]	1483.3, 1486.5	1489.3	...	1.0?	1.8	1.8
C IV	1548.2, 1550.8	1549.4	4.0	3.8	6.6	9.2
He II	1640.4	1639.7	1.3	1.0	1.3	1.7
O III]	1660.8, 1666.1	1663.7	2.2	1.7	2.3	2.9
N III]	1746.8, 1748.6, 1749.6	1750.5	2.0	1.6	2.3	2.6
	1752.1, 1753.9	...	...	...	...	...
Si II	1808.8, 1816.9, 1817.4	1817.4	1.1	0.7	0.6	1.3
Si III]	1892.0	1893.2	2.5[c]	3.0	3.6	3.5
C III]	1906.7, 1908.7	1907.4	4.8[c]	6.3[c]	7.8[c]	8.7[c]
[O III] + C II]	2320.9, 2323.5, 2324.7	2329.4	4.8[c]	4.8	4.4	8.2
	2325.4, 2326.9, 2328.1	...	...	...	...	...
[O II]	2470.3	2472.4	2.8	2.8	2.7	4.0
Mg II	2795.5, 2802.7	2800.4	4.7[c]	6.9	4.4	5.5
O III	3132.9	3128.5	...	...	0.9	0.8
He II	3203.1	3190.6	...	...	2.6	2.5

[a] Wavelengths have been averaged.
[b] Flux is in units of 10^{-12} ergs cm^{-2} s^{-1}.
[c] Saturated emission feature.

and emission-line fluxes were 1.5–2 times stronger compared with the levels shown in Figure 2*b* (1983 May), except Mg II λλ2795, 2803, which declined in intensity. The most dramatic changes in the ultraviolet took place between 1986 October (Fig. 2*c*) and 1991 May (Fig. 2*d*), where the UV continuum flux distribution substantially increased (~1.5 times) toward shorter wavelengths. Moreover, emission-line fluxes of O I, C II, C IV, O III], Si II, C II] + [O III], and [O II] were ~1.5–2 times greater compared with levels of 1986 October (Fig. 2*c*). Notice the increased strength of C IV λλ1548, 1550, C III] λλ1907, 1909, and [O III] + C II] λλ2320–2328 in Figure 2*d* (1991 May).

The overall UV continuum flux distribution of the H II region declined slightly from 1981–1985 then increased toward both shorter and longer wavelengths until 1991 May. In addi-

TABLE 2B

LOW-RESOLUTION NE JET ULTRAVIOLET SPECTRA OF R AQUARII

ION	λ(lab) (Å)	λ(IUE)[a] (Å)	FLUX[b] SWP 20068, LWR 16016	SWP 29989, LWP 9814	SWP 32645, LWP 12404	SWP 36397, LWP 15662
N V	1238.8, 1242.8	1239.4	8.6	11.5	15.2	14.9
O I	1301.1, 1304.9, 1306.0	1304.9	11.7	9.6	10.3	10.5
C II	1334.5, 1335.7	1334.2	7.9	13.8	14.7	16.5
Si IV	1393.8	1392.2	5.4	9.1	10.1	11.7
O IV]	1397.2, 1399.8, 1401.1	1400.3	8.1	11.9	15.4	16.6
	1404.8, 1407.3	...	...	...	...	...
N IV]	1483.3, 1486.5	1484.3	...	9.8	10.0	9.9
C IV	1548.2, 1550.8	1547.4	14.6	30.8[c]	39.6[c]	40.5[c]
He II	1640.4	1638.2	4.0	8.0	10.0	9.5
O III]	1660.8, 1666.1	1663.0	7.2	13.2	15.0	16.5
N III]	1746.8, 1748.6, 1749.6	1749.6	6.2	10.6	11.7	13.2
	1752.1, 1753.9	...	...	...	...	...
Si II	1808.0, 1816.9, 1817.4	1815.3	...	4.4	5.5	7.2
Si III]	1892.0	1891.5	5.5	12.3	15.5	15.7
C III]	1906.7, 1908.7	1904.8	15.7[c]	27.5[c]	30.4[c]	33.8[c]
[O III] + C II]	2320.9, 2323.5, 2324.7	2328.7	13.2	38.4	51.7	51.2
	2325.4, 2326.9, 2328.1	...	...	...	...	...
[O II]	2470.3	2472.3	8.0	14.4	20.3	20.2
Mg II	2795.5, 2802.7	2799.2	14.2	18.5	25.9	23.9
O III	3132.9	3126.0	...	2.2	3.1	2.2
He II	3203.1	3186.0	...	...	8.1	6.6

[a] Wavelengths have been averaged.
[b] Flux is in units of 10^{-13} ergs cm^{-2} s^{-1}.
[c] Saturated emission feature.

TABLE 2C

LOW-RESOLUTION SW JET ULTRAVIOLET SPECTRA OF R AQUARII

ION	λ(lab) (Å)	λ(*IUE*)[a] (Å)	FLUX[b] SWP 37914	FLUX[b] SWP 41706
N v	1238.8, 1242.8	1240.7	1.5	1.1
O i	1301.1, 1304.9, 1306.0	1305.4	0.6	0.3
C ii	1334.5, 1335.7	1335.6	3.8	3.3
Si iv	1393.8	1394.1	2.5	1.9
O iv].....	1397.2, 1399.8, 1401.1 1404.8, 1407.3	1401.4	2.0	1.9
N iv].....	1483.3, 1486.5	1491.9	1.3?	1.0?
C iv	1548.2, 1550.8	1548.4	8.0	6.4
He ii	1640.4	1640.5	0.8	0.5
O iii].....	1660.8, 1666.1	1665.4	2.7	2.0
N iii].....	1746.8, 1748.6, 1749.6 1752.1, 1753.9	1752.0 ...	2.4 ...	2.5 ...
Si ii.....	1808.0, 1816.9, 1817.4	1817.1	0.5	...
Si iii].....	1892.0	1884.6	2.2	3.1
C iii].....	1906.7, 1908.7	1907.0	10.3[c]	9.4[c]

[a] Wavelengths have been averaged.
[b] Flux is in units of 10^{-13} ergs cm^{-2} s^{-1}.
[c] Saturate emission feature.

tion, most emission-line intensities have increased by factors of ~2–3 compared to earlier values in 1980 November. These spectra indicate that the central H II region or feature A are increasing in excitation or that the emitting volume is increasing. We believe the emergence of N v λλ1238, 1240 around 1986 October, coupled with the fact that both N v and He II line fluxes have steadily increased in intensity, argues for higher excitation conditions in feature A. The reason is that since the 10″ × 20″ *IUE* large aperture receives flux from both the H II region and feature A (see Fig. 2 of Michalitsianos & Kafatos 1988), and N v and He II were previously detected in the NE jet (Kafatos et al. 1986), these high-excitation lines most likely originate in feature A instead of the central H II region. Unfortunately, no *IUE* spectra exist beyond 1991 December; therefore, we cannot comment on whether these high-ionization lines are still present in the UV spectrum of R Aqr.

Low-resolution UV spectra of the NE jet are shown in Figures 3*a*–3*d*. The *IUE* spectrum taken in 1983 May (Fig. 3*a*) displays emission lines of C IV λλ1548, 1550, C III] λλ1907, 1909, [O III] + C II] λλ2320–2328, [O II] λ2470, and Mg II λλ2795, 2803 and an ultraviolet continuum flux which rises with decreasing wavelength. One interesting feature to note in Figure 3*a* is the first detection of N v λλ1238, 1242 in the NE jet. The most radical changes in the UV spectra of the NE jet took place in 1986 December (Fig. 3*b*), where the continuum flux distribution increased considerably in the short- and long-wavelength regions and emission lines of C II, N IV], C IV, Si III], [O III] + C II], [O II], Mg II, and O III were approximately 1.5–2 times greater than corresponding levels in 1983 May (Fig. 3*a*). Figure 3*c* (1987 December) exhibits a moderate ultraviolet continuum flux which rises toward shorter wavelengths and a variety of emission lines which are slightly stronger than the line intensities found in Figure 3*b* (1987 December). The UV continuum flux and emission-line fluxes remained essentially constant through 1989 June, as can be seen in Figure 3*d*.

The overall UV continuum flux distribution of the NE jet increased by a factor of ~2–3 over the *IUE* observation period (1982–1989), and the emission-line intensities have increased 2–3 times compared to levels in 1983 May (Fig. 3*a*). The overall increase in the UV continuum flux and in virtually all emission-line intensities provides evidence, as indicated earlier, that the excitation of the NE jet continues to increase, or perhaps the emitting volume is expanding. The increased intensities of N v λλ1238, 1242, N IV] λλ1483, 1487, and He II λ1640 over the period of *IUE* observations indicates that high-excitation conditions exist in features A and B, consistent with the findings of Kafatos et al. (1986), Michalitsianos et al. (1986), and Hollis et al. (1991). Again, the lack of more recent data (the last low-resolution *IUE* spectrum was taken in 1991 December and was overexposed) makes it difficult to know the present excitation conditions in the NE jet.

Low-resolution SWP (λλ1200–2000) *IUE* spectra of the SW jet are shown in Figures 4*a* and 4*b*. Figure 4*a* (1989 December) and Figure 4*b* (1991 May) both contain a weak UV continuum with several strong emission lines of C II, Si IV + O IV], C IV, O III], N III], and C III]. The line intensities in the earlier spectrum (Fig. 4*a*) are approximately ~1.2–4 times greater compared to levels in the later spectrum (Fig. 4*b*). The decrease in emission-line flux indicates that the SW jet has declined in intensity between 1989 December and 1991 May. Notice the weakness of N v λλ1238, 1242 and He II λ1640 in the SW jet compared to the values found in the NE jet (see Tables 2B and 2C).

The temporal UV variability of the H II region and NE jet of R Aqr are shown in Figures 5*a*–5*h*, where the total integrated UV flux and individual line fluxes are plotted as a function of time. The line fluxes in Figures 5*c*–5*h* are shown in order of increasing wavelength and represent the temporal variations of O I λλ1302–1306, C II λλ1334, 1335, C IV λλ1548, 1550, O III] λλ1660, 1666, N III] λλ1747–1753, [O III] + C II] λλ2320–2328. We cannot discern any periodic behavior in the far-UV emission of either the H II region of the NE jet. A Fourier transform method was implemented to ascertain if any periodicity exists in the data. However, since the data set is small and irregularly spaced, this method proved fruitless. Using a smaller data set, Kafatos et al. (1986) found an ~1.5 yr period in the NE jet. We discount this value because the period was determined from a

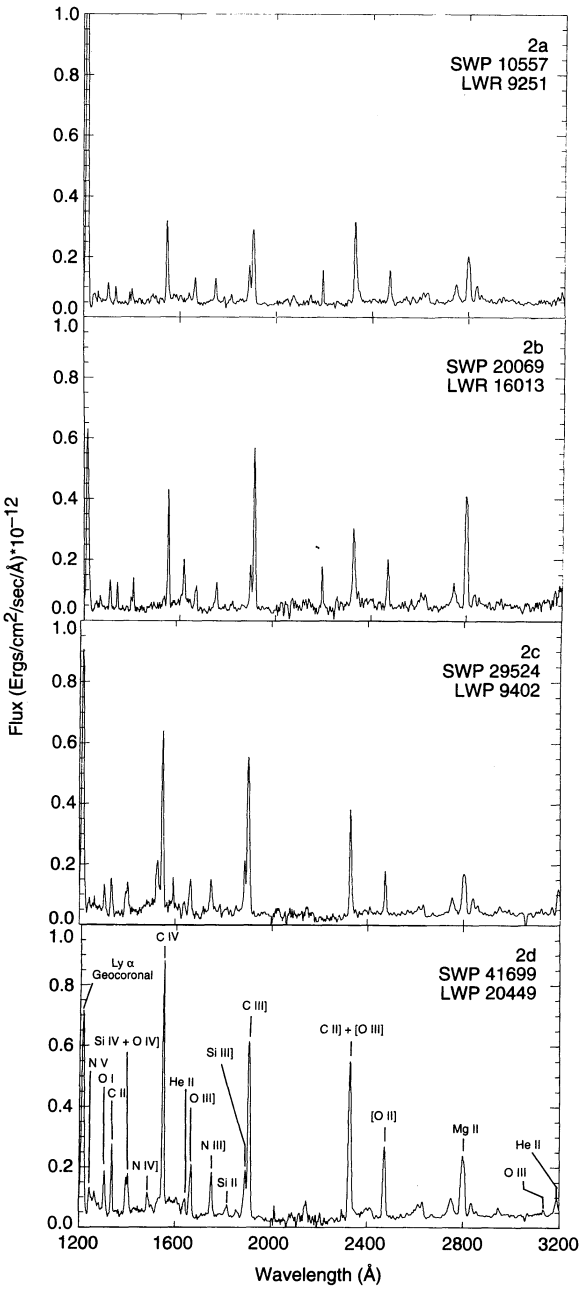

FIG. 2.—Low-resolution *IUE* spectra of the H II region (features C1, C2, A, and A′) of R Aquarii obtained between 1980 November and 1991 May in the SWP ($\lambda\lambda$1200–2000) and LWP/LWR ($\lambda\lambda$2000–3200) wavelength regions. Notice the increase in the UV continuum flux and emission-line intensities over this timespan.

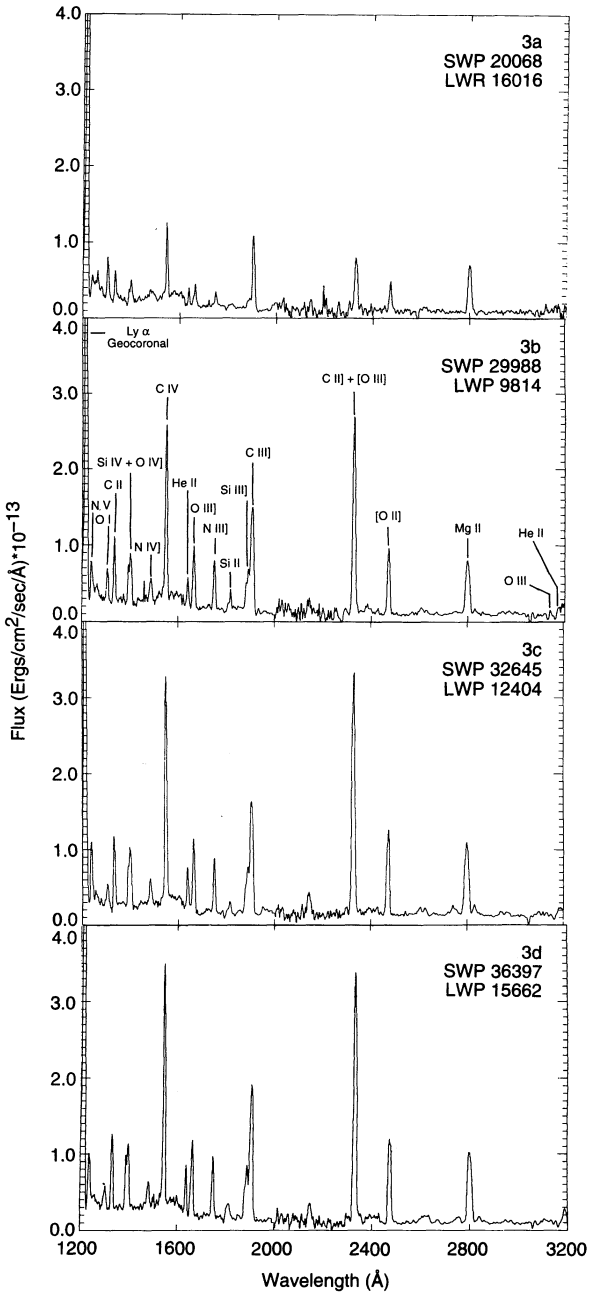

FIG. 3.—Low-resolution *IUE* spectra of the NE jet (features A, B, and D) of R Aquarii obtained between 1983 May and 1989 June in the SWP ($\lambda\lambda$1200–2000) and LWP/LWR ($\lambda\lambda$2000–3200) wavelength range. Note the increase in the UV continuum flux and emission line intensities over this 7 yr period.

4 yr data set. These plots also provide evidence that the far-UV emission does not vary with the 386 day pulsation period of the Mira.

The temporal variability plots suggest the H II and NE jet regions are increasing in intensity. The total integrated UV line flux in the SWP wavelength region was obtained by measuring the UV flux between 1225–1900 Å, excluding Lyα λ1216 geocoronal line emission and C III] $\lambda\lambda$1907, 1909 because they are often saturated. Similarly, the integrated flux throughout the LWP/LWR (2000–3200 Å) wavelength range was also obtained. Between 1979 January (~JD 2,443,850) and 1985 January (~JD 2,446,100) the total UV flux and individual emission line intensities in the H II region declined, reaching a minimum around 1985 January (~JD 2,446,200), after which the total UV flux and emission-line fluxes began to increase and have continued in an upward trend until 1991 December (~JD 2,448,600). In addition, all temporal variability plots confirm that the NE jet has continually increased in intensity since the first *IUE* observation in 1982 May.

Figures 6*a*–6*f* show various ionization stages of the same element (e.g., O I, O III], O IV], C II, C III], C IV, Si II, Si III], and Si IV) plotted versus time for the H II region and NE jet. All

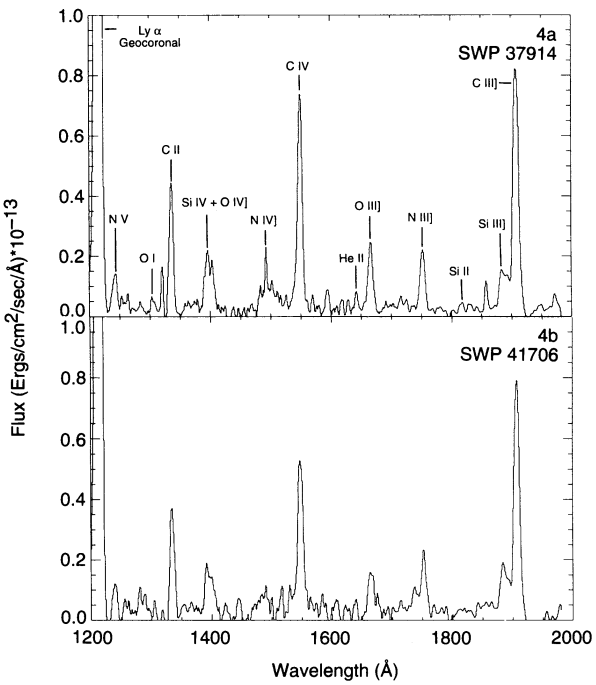

FIG. 4.—Low-resolution *IUE* spectra of the SW jet (feature A′) of R Aquarii obtained between 1989 December and 1991 May in the SWP ($\lambda\lambda$1200–2000) wavelength region. Notice the decrease in the UV continuum flux and emission-line intensities.

ionization stages for each element in the NE jet correlate (i.e., have similar minima and maxima) at approximately the same times with each other remarkably well. This provides evidence that the excitation source in the NE jet is exciting all ions equally at a constant ionization temperature. The ions of the same element in the H II region (see Figs. 6*d*–6*f*) show some correlation, mainly in the later data ($\geq$JD 2,447,500). The lack of clear correlations in the H II region may result from the *IUE* 10″ × 20″ large aperture receiving combined emission from both the H II region and feature A.

In Figures 7*a*–7*f*, successive ionization levels of carbon, nitrogen, oxygen, and silicon are plotted against each other to provide insights into the nature of the ionizing source in the NE jet. The line fluxes in the NE jet are generally proportional to each other for a variety of ionization states. Assuming these ions are formed in the same region, this linear relationship may indicate that the ions are being excited equally at all ionization levels. This would favor an increase in the emission measure $n_e^2 L^3$ at a constant ionization temperature. For example, if the ionization state of the gas were increasing, one would expect to observe more O IV] at the expense of O III], assuming again that the ions form in the same region. Since this is not the case, the total luminosity in each emission line may be increasing at a constant ionization temperature, perhaps as a result of an expanding emitting volume.

3.2. *Nebular Parameters*

The Si III] $I(\lambda1882.7)/I(\lambda1892.0)$ density-sensitive diagnostic ratio (Nussbaumer 1986) was used to obtain an estimate of the electron density (n_e) in the H II region and NE jet. These line intensities imply a volume-averaged density of 4×10^5 cm^{-3} for the nebulosities surrounding the central star region and an $n_e \sim 6 \times 10^4$ cm^{-3} for the nebulosities in the NE jet. The estimate for the H II region is lower than most other estimates of $n_e \geq 10^6$ cm^{-3} (Wallerstein & Greenstein 1980; Michalitsianos, & Kafatos 1982; Hollis et al. 1991), while the electron density for the NE jet is higher than the values of $n_e \leq 10^4$ cm^{-3} found by Hollis et al. (1985), Michalitsianos et al. (1988), and Hollis et al. (1991). Another diagnostic for determining the electron density is the [O III] forbidden to O III] semiforbidden density-dependent line ratio of $I(\lambda2321.0)/I(\lambda1660.8+\lambda1666.1)$ (Nussbaumer & Storey 1981). This line ratio yielded a value for the electron density in the H II region of $n_e \sim 9 \times 10^5$ cm^{-3} and is in closer agreement with the estimates found by the authors listed above. The n_e estimates obtained using the O III line ratio were taken from one high-resolution spectrum, whereas estimates using the Si III] ratio are more reliable because the line ratios were obtained from two high-resolution spectra taken over a 4 yr time period.

Electron temperatures (T_e) for the H II region and NE jet were obtained using the temperature-dependent C II line ratio $I(\lambda2325)/I(\lambda1335)$ (Hayes & Nussbaumer 1984). Throughout the *IUE* observations, the H II region T_e appeared constant, with a temperature range of $16{,}000 \leq T_e \leq 22{,}500$ K. These values are higher than other estimates of $T_e = 6600$–$18{,}000$ K (Wallerstein & Greenstein 1980; Michalitsianos et al. 1980; Michalitsianos et al. 1988), although there is an overlap in the 16,000–18,000 K range by all authors. The T_e values for the NE jet displayed some curious behavior. Between 1982 May and 1983 December the T_e value was found to be $\geq$26,000 K, then between 1986 December and 1989 June the electron temperature decreased to a value of $T_e \leq 18{,}200$ K. This value is in disagreement with the estimate determined by Hollis et al. (1991) of $T_e \sim 26{,}000$ K from optical observations obtained in 1989 November. The T_e value in the NE jet appears to be decreasing, while the UV line intensities and continuum flux have increased with time. Since the emission measure is proportional to the cube of the line-emitting region and the square of the electron density, this may indicate an increasing emitting volume or electron density, or perhaps both are responsible for the rise in UV line intensities.

The absolute intensities of the UV lines and our estimates of n_e and T_e were used to estimate the characteristic length of the nebular emitting region. In this paper, the nebular emitting region was calculated for the H II region and NE jet using carbon, oxygen, and silicon line intensities. For densities up to $\sim 5 \times 10^{10}$ cm^{-3} the semiforbidden line strengths are proportional to $n_e^2 L\Omega$, where L is the path length through the emitting region and Ω is the solid angle of the region observed from Earth (Osterbrock 1974). The expression for the line strength is proportional to $n_e^2 L^3/d^2$ for a spherical region:

$$I = \frac{n_e^2 L^3}{d^2 \sqrt{T_e}} e^{-\Delta E/kT_e} N_{A,Z} \left(\frac{n_A}{n_{A\odot}} \right), \quad (1)$$

where d is the distance from the Earth, n_e is the electron density, T_e is the electron temperature, ΔE is the line excitation energy, $N_{A,Z}$ is the elemental ionic abundance A with charge Z, n_A is the chemical abundance with atomic number A, and $n_{A\odot}$ is the solar abundance. We assume solar abundances $\Sigma_{\text{all}\,Z} N_{A,Z} = 1$ (Michalitsianos et al. 1980). If the region is in the form of streams, rings, or a disk, the geometrical effects have to be taken into account. In general, equation (1) can be written with a factor f_g, where $f_g < 1$ depending on the geometry of the region relative to the line of sight (Kafatos, Michalitsianos, & Feibelman 1982). The factor f_g is equal to unity in the spherical case, where L is always understood to be

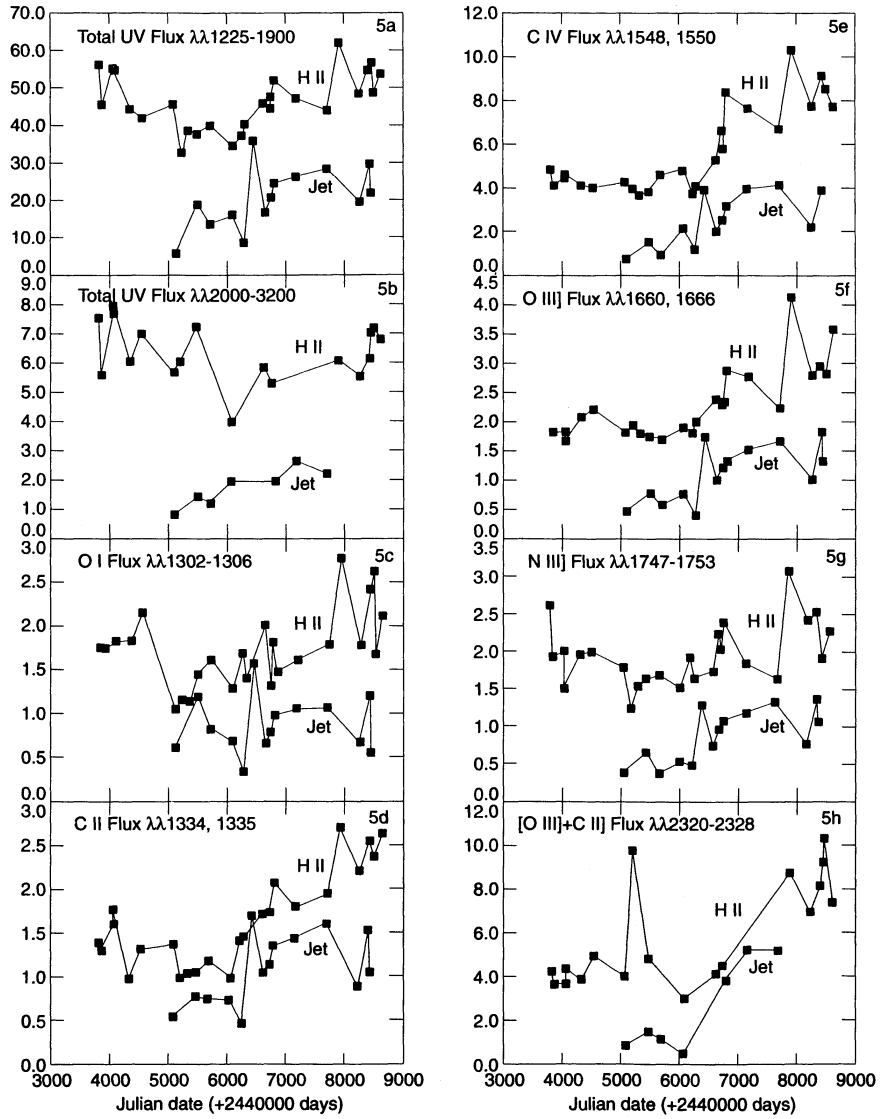

FIG. 5

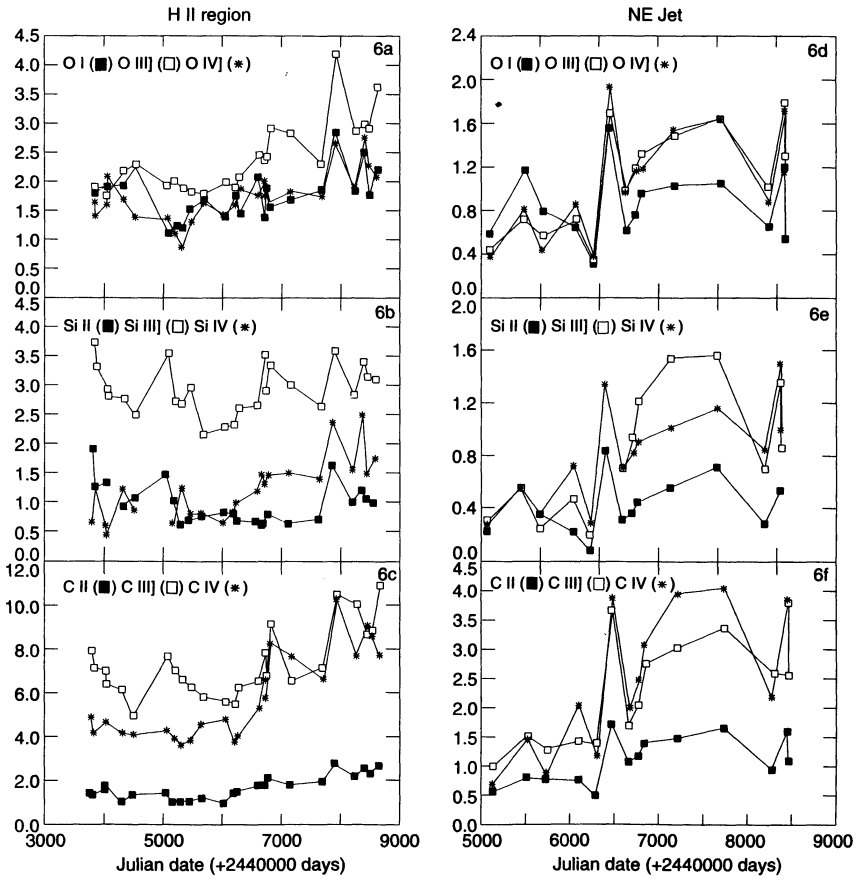

FIG. 6

FIG. 5.—(*a*) Total UV flux (λλ1225–1900), (*b*) Total UV flux (λλ2000–3200), (*c*) O I λλ1302–1306, (*d*) C II λλ1334, 1335, (*e*) C IV λλ1548, 1550, (*f*) O III] λλ1660, 1666, (*g*) N III] λλ1747–1753, and (*h*) [O III] + C II] λλ2320–2328 absolute fluxes of the H II region and NE jet plotted as a function of time. Note the increase in emission-line intensities for the H II region and NE jet as a function of time. Fluxes are in 10^{-12} ergs cm^{-2} s^{-1} Å^{-1}.

FIG. 6.—(*a, d*) O I λλ1302-1306, O III] λλ1660, 1666, O IV] λλ1397–1407, (*b, e*) Si II λ1816, Si III] λ1892, Si IV λ1393, (*c, f*) C II λλ1334, 1335, C III] λλ1907, 1909 (often saturated), C IV λλ1548, 1550 low-resolution absolute line intensities of the H II region and NE jet plotted against time. Filled squares represent the lowest ionization stage for each element (O I, Si II, C II); open squares represent the next stage (O III], Si III], C III]), and the highest ionization stage is represented by an asterisk (O IV], Si IV, C IV). Note the close correlation between the line intensities in the NE jet. Line intensities are in 10^{-12} ergs cm^{-2} s^{-1} Å^{-1}.

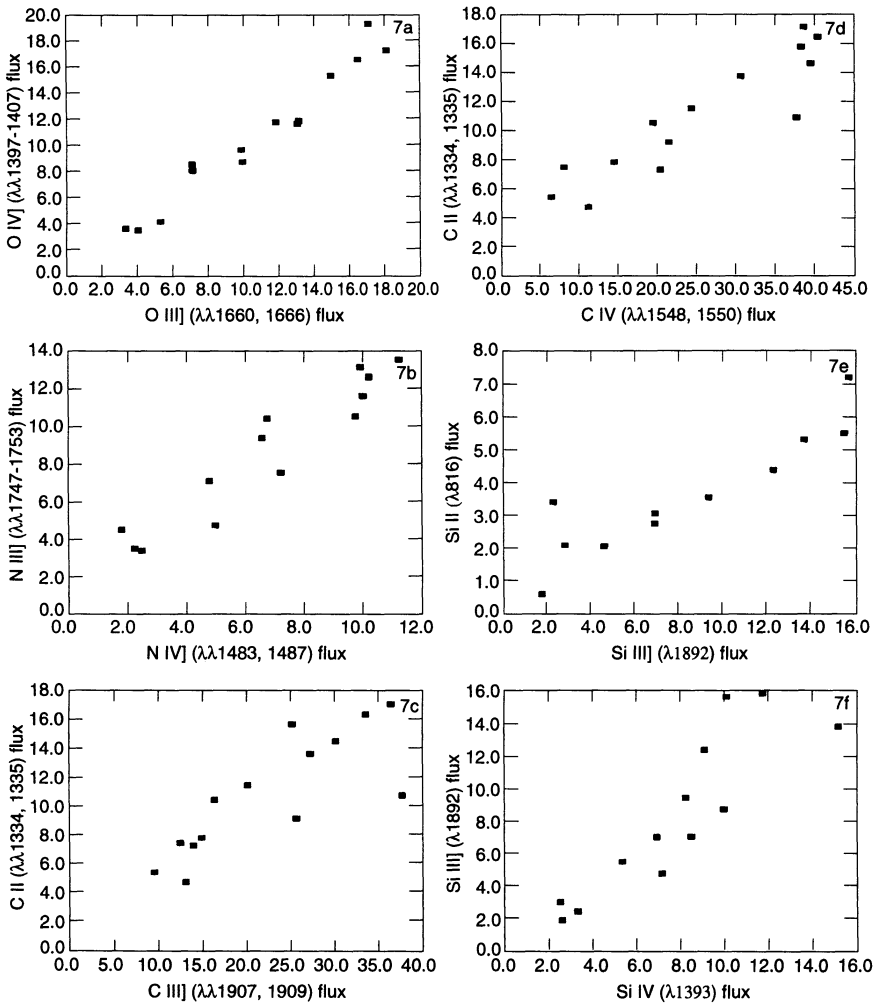

FIG. 7.—(*a*) O IV] λλ1397–1407 vs. O III] λλ1660, 1666, (*b*) N III] λλ1747–1753 vs. N IV] λλ1483, 1487, (*c*) C II λλ1334, 1335, vs. C III] λλ1907, 1909 (often saturated), (*d*) C II λλ1334, 1335 vs. C IV λλ1548, 1550, (*e*) Si II λ1816 vs. Si III] λ1892, (*f*) Si IV λ1816 vs. Si IV λ1393 low-resolution emission-line fluxes of the R Aqr NE jet (features A, B, and D). Notice the linear relationship between the successive ionization stages. Fluxes are in 10^{-13} ergs cm^{-2} s^{-1} Å^{-1}.

the largest characteristic size of the region (e.g., the diameter of the sphere or diameter of the disk). With $f_g = 1$ and corresponding values of $d = 250$ pc, $n_e = 4 \times 10^5$ cm^{-3}, and $T_e = 20{,}000$ K, the line-emitting region of the H II region was found to be $L = 6.3 \times 10^{14}$ cm. Values of $d = 250$ pc, $n_e = 6 \times 10^4$ cm^{-3}, and $T_e = 22{,}000$ K were substituted in equation (1) and yielded a value of $L = 1.5 \times 10^{15}$ cm for the NE jet. These values should be considered as lower limits. A summary of the nebular parameters for R Aqr can be found in Tables 3 and 4.

TABLE 3

AVERAGE NEBULAR PARAMETERS FOR R AQUARII

Region	n_e (cm^{-3})	T_e (K)	L (cm)
H II	4×10^5	19,000	6.3×10^{14}
NE Jet	6×10^4	≥26,000[a]	1.5×10^{15}
		18,000 ≤ [b]	...
SW Jet	4×10^2 [c]	33,000[c]	...

[a] Between 1982 May and 1983 Dec.
[b] Between 1986 Dec and 1989 Jun.
[c] From optical line ratios (Hollis et al. 1991).

TABLE 4

TIME EVOLUTION OF THE NEBULAR PARAMETERS L AND n_e FOR R AQUARII

Observation Date	L (cm)	n_e (cm^{-3})
H II Region:		
1979 Jan 1	6.02×10^{14}	...
1980 Nov 8	...	9.0×10^5
1982 Oct	...	5.0
1983 May 25.....	5.90	...
1986 Oct 27.....	6.35	...
1987 Jun 4	...	2.0[a]
1990 Dec 3.....	6.70	3.5
1991 Dec 13	6.98	...
1992 Dec 26	...	3.0[a]
NE Jet:		
1982 May 7.....	1.16×10^{15}	...
1986 Oct 27.....	...	6.0×10^4
1986 Dec 29	1.67	...
1989 Jun 5	1.83	...

[a] Saturated line ratio.

3.3. *Properties of the Mira and Orbit*

The properties of the Mira variable are presented in this section. Assuming $M_1 \sim 2\,M_\odot$, $M_2 \sim 1\,M_\odot$ (Wallerstein 1986) and a 44 yr orbital binary period, Kepler's law was used to determine a value for the semimajor axis of the orbit $a \sim 2.7 \times 10^{14}$ cm. This value is comparable to the emission path length of the H II region. From the historical light curve provided by the AAVSO (Fig. 8), the 387 day Mira varies in visual magnitude between $\Delta m_V = 6$–12 mag. Since the 1930s outburst, the Mira has maintained almost constant minima and maxima. However, in the mid-1970s the minima and maxima declined by $\sim$2 mag, possibly indicating obscuration in the visual region (Whitelock et al. 1983). Since 1978, the Mira light has increased by 2 mag, suggesting that the obscuration is no longer present. A radius has been estimated at 250–300 $R_\odot$ (Kafatos & Michalitsianos 1982; Burgarella, Vogel, & Paresce 1992) and a temperature of 2800 K (Anandarao & Pottasch 1986) for the M7 III Mira.

3.4. *Properties of the Secondary*

The number of ionizing photons needed to ionize the H II region surrounding the binary star containing a hot subdwarf or white dwarf was calculated using the Strömgren relation (Spitzer 1978), where we assumed that the H II region is the Stromgren sphere. With calculated values for the H II region of $n_e \sim 4 \times 10^5$ cm^{-3} and $T_e = 20{,}000$ K, the number of hydrogen ionizing photons or Lyman continuum photons required to ionize the H II region (i.e., features C_1, C_2, A, and A′) was found to be $N_i(\mathrm{H\ I}) = N_i(h\nu \geq 13.6\ \mathrm{eV}) = 3.2 \times 10^{42}\ \mathrm{s}^{-1}$.

TABLE 5

HOT COMPONENT PARAMETERS FOR ASSUMED EFFECTIVE TEMPERATURES T_*

	VALUE[a]	
PARAMETER	$T_* = 50{,}000$ K	$T_* = 100{,}000$ K
R_* ($R_\odot$).....	0.003	0.001
L_* ($L_\odot$).....	0.05	0.04

[a] Values based on the number of Lyman continuum photons required to ionize the H II region.

Hummer & Mihalas (1970) determined that the overall number of ionizing photons (beyond the Lyman limit) in their stellar models is not greatly different from the estimated number of photons that arise from a blackbody. Since most of the energy emitted by the central star is in the far-UV, blackbody formulae (Allen 1976) were utilized to estimate R_* and L_*, the radius and luminosity of the secondary star. These values were then used to determine whether the size and luminosity of the secondary are consistent with the number of ionizing photons N_i ($h\nu \geq 13.6$ eV) required to photoionize the nebula. Table 5 lists these values at two different effective temperatures ($T_* = 50{,}000$ K and 100,000 K) for the central star.

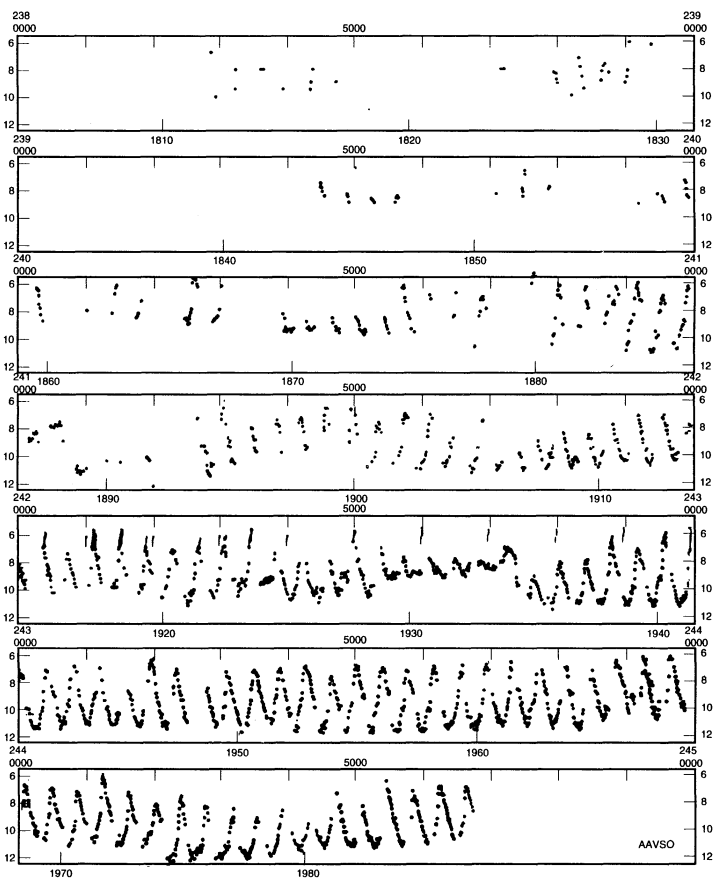

FIG. 8.—Visual light curve of 387 day Mira variable in R Aquarii from 1811 to 1987 (AAVSO data, kindly provided by J. Mattei). Note the outburst that occurred between 1928 and 1935 and the steady increase in visual light since 1978.

The results from Table 5 provide evidence that, in the case of photoionization by the secondary, the secondary star is a small white dwarf. However, we believe that $T_* = 100{,}000$ K is a upper limit for the hot component in R Aqr because the overall state of ionization of this system (e.g., Kafatos et al. 1986) is one of the lowest for symbiotic stars. Moreover, we obtain an unreasonably small radius for the hot star, providing an additional argument that T_* is close to $\sim 50{,}000$–$60{,}000$ K than 10^5 K.

The He II $\lambda 1640$ modified Zanstra method was used to estimate the effective temperature of the hot component. The temperature of the hot star can be determined from the He II emission, assuming that the nebula absorbs all radiation shortward of 228 Å (He II Lyman continuum limit) and the star emits as a blackbody (Pottasch 1984). In this method, the He II $\lambda 1640$ line intensity is divided by the underlying continuum (assumed stellar) at the same wavelength (Murset et al. 1991). This method depends on the intensity of the He II $\lambda 1640$ Baα transition, the recombination coefficient for the nth level $\alpha(n)$, the numerical value of the integral used in the Zanstra method $G_4(T)$, and the electron temperature. Assuming $T_e = 20{,}000$ K for the H II region, we used the following equation to determine the effective temperature T_*:

$$\frac{F(\lambda 1640)}{F_\lambda} = 1.3 \times 10^{-11} \frac{\alpha(2)}{\alpha(3)} (e^{h\nu/kT_*} - 1) T_*^3 G_4(T) . \quad (2)$$

Our calculations yield an effective temperature of $T_* \approx 60{,}800$ K for the hot star. The resultant effective temperature of the hot component of R Aqr may be slightly higher, since the underlying continuum at $\lambda 1640$ may have a nebular component from free-free and free-bound emission. This estimate is consistent with the number of ionizing photons $\sim 10^{42}$ s^{-1} calculated above. The value of T_* obtained here is still higher than the most recent estimate of $T_* \sim 40{,}000$ K (Burgarella et al. 1992), but it is in agreement with previous estimates of $T_* \geq 50{,}000$ K (Michalitsianos et al. 1980; Kaler 1981; Kafatos & Michalitsianos 1982). We conclude that if the origin of the ionizing radiation is a stellar continuum, then the implied hot star has a temperature of $50{,}000 \text{ K} \lesssim T_* \lesssim 60{,}000$ K and a radius of $R_* \simeq 10^8$ cm.

3.5. *Accretion Disk Parameters*

Alternatively, the photoionizing radiation may arise from an accretion disk and its inner boundary layer region. The relations derived by Bath et al. (1974), Lynden-Bell & Pringle (1974), and Tylenda (1977) are used to estimate the various accretion parameters. The only assumption made in these calculations is that the observed blackbody continuum arises from the boundary-layer accretion disk, with a temperature T_{bl} that surrounds the secondary star.

For temperatures $T_{bl} = 40{,}000$ K (*lower limit*) and $T_{bl} = 100{,}000$ K (*upper limit*), the relevant corresponding relationships are

$$R_* \geq 5.77 \left(\frac{T_{bl}}{10^5 \text{ K}}\right)^{-3/2} \left[\frac{N_i(\text{H I})}{f * 10^{45} \text{ s}^{-1}}\right]^{1/2} \times 10^9 \text{ cm} ,$$

$$\dot{M}_{-8} M_* \geq 3.22 \left(\frac{T_{bl}}{10^5 \text{ K}}\right)^{-1/2} \left[\frac{N_i(\text{H I})}{f * 10^{45} \text{ s}^{-1}}\right]^{1/2} ,$$

$$L_d \geq 5.91 \left(\frac{T_{bl}}{10^5 \text{ K}}\right) \left[\frac{N_i(\text{H I})}{f * 10^{45} \text{ s}^{-1}}\right] L_\odot ,$$

$$\frac{L_T}{L_{Edd}} \geq 4.95 \times 10^{-4} M_*^{-1} \left(\frac{T_{bl}}{10^5 \text{ K}}\right) \left[\frac{N_i(\text{H I})}{10^{45} \text{ s}^{-1}}\right] ,$$

$$\beta \leq 2.6 \times 10^{-5} M_* \left(\frac{T_{bl}}{10^5 \text{ K}}\right)^{3/2} \left[\frac{N_i(\text{H I})}{f * 10^{45}}\right]^{-1/2} ,$$

where R_* is the radius of the secondary, $\dot{M}_{-8} = M/10^{-8} M_\odot$ yr^{-1} is the accretion rate onto the secondary, M_* is the mass of the secondary, N_i is the number of Lyman continuum photons ($h\nu \geq 13.6$ eV) emitted from the boundary layer, f is found from tables of blackbody functions, L_d is the luminosity of the disk, L_T is the total luminosity (disk + boundary layer), $L_{Edd} = 1.3 \times 10^{38} (M/M_\odot)$ ergs s^{-1} is the Eddington luminosity, and β is the efficiency of the accretion. Assuming $M_* = 1\ M_\odot$ and $N_i = 3.2 \times 10^{42}$ s^{-1}, the obtained accretion disk parameters are presented in Table 6.

From the calculated values of R_* and L_* in Table 6, it is obvious that the secondary star in R Aqr cannot be a solar-type main sequence-star. Under the assumption of an accretion disk/boundary layer providing the ionizing radiation, and for a boundary layer temperature of $T_{bl} = 100{,}000$ K, the derived radius in Table 6 indicates that the secondary is a hot subdwarf. The results in Tables 5 and 6 indicate that if the hot star itself provides the photoionization, then it is approximately an order of magnitude smaller than the corresponding size estimated if the source of the photoionizing flux were the boundary layer of the accretion disk.

The theoretical results in Tables 5 and 6 are subject to *IUE* uncertainties, since the absolute emission-line flux is affected by calibration errors and signal-to-noise ratio. The estimates for the line-emitting region L are derived from the observed line intensities which are subject to uncertainties of $\sim 4\%$–5% for the strongest lines and $\sim 10\%$–15% for the weaker lines. The size L is then used to calculate the number of ionizing photons from the Strömgren relation. This calculation results in large uncertainties, since the relative errors are related by $\Delta N_i/N = 3\Delta L/L$ for N_i. Therefore, the values in Tables 5 and 6 should be taken as estimates to within a factor of 3–5 of the actual properties of the ionizing source.

4. DISCUSSION AND CONCLUSIONS

The complete set of *IUE* ultraviolet spectra of the symbiotic star R Aqr has been analyzed. In this section, the interpretations and conclusions of our ultraviolet observations are given.

The total UV flux and emission-line intensities in the NE jet have been increasing over the last decade, as can be seen in Figures 3*a*–3*d* and Table 2B. Over the time period of *IUE* NE jet observations (1982–1989), the UV continuum flux increased by factors of 2–3, and emission-line intensities increased by 2–3

TABLE 6

ACCRETION DISK PARAMETERS FOR R AQUARII

PARAMETER	VALUE[a]	
	$T_{bl} = 40{,}000$ K	$T_{bl} = 100{,}000$ K
R_* ($R_\odot$)	0.04	0.006
$\dot{M}_{-8}$ ($M_\odot$ yr^{-1})	1.2×10^{-10}	1.0×10^{-11}
L_d ($L_\odot$)	0.04	0.03
L_T/L_{Edd}	3.2×10^{-6}	2.3×10^{-6}
β	4.9×10^{-5}	3.8×10^{-4}

[a] Values based on the number of Lyman continuum photons required to ionize the H II region.

times. Moreover, the emission-line fluxes and total integrated UV flux plotted as a function of time in Figures 5*a*–5*h* clearly exhibit a trend of increasing emission with time. The emission-line intensities in the SW jet, on the other hand, have declined by ~1.5 times between 1989 December and 1991 May. The detection of the high-excitation emission lines N v λλ1238, 1242 and He II λ1640 in both the NE and SW jets provides evidence of highly excited regions with ionizing temperatures $\gtrsim$65,000 K.

The elevation in the N v and He II fluxes argues that higher excitation conditions may be occurring in the NE jet as a function of time. However, T_e calculations using the C II temperature-dependent line ratio indicate that the temperature of the gas is declining. In addition, the line-emitting region L is increasing (see Table 4), consistent with a decreasing T_e. If the temperature of the gas is decreasing and the line-emitting region is becoming larger, this may indicate a region that is expanding as the shocked region expands and becomes more dilute (see below).

The UV observations may be consistent with a model for the NE and SW jets in which a shock is the primary source of excitation. This shock may form as the stellar wind from the hot star or a bipolar wind from an accretion disk collides with condensations of matter, i.e., features A, B, and D (Solf 1992). *HST* FOC observations by Paresce et al. (1991) found a continuous and highly collimated stream of material extending in the NE direction. Further FOC observations by Paresce & Hack (1944) found that the NE jet is highly collimated within 15 AU of the Mira, placing it well within the binary orbit. In addition, from emission-line ratios, they determined that most of the emission in the jet is due to shock-driven material colliding with the material from earlier mass ejection events. These high-resolution observations provide strong evidence that the jet is continuous and highly collimated.

Our far-UV results indicate that a energetic stellar wind most likely originates from an accretion disk. An accretion disk could have formed in the mid-1970s near periastron as material from the Mira overflowed its Roche lobe and formed an accretion disk around the hot component (Kafatos & Michalitsianos 1982). The far-UV temporal variability plots in Figures 5*a*–5*h* indicate that the far-UV emission of the NE jet does not vary on a 386 day period or any multiple of the 386 day pulsation period of the Mira. Therefore, we do not believe that the Mira is intimately connected to the far-UV emission in the NE jet. Moreover, the *IUE* spectra and temporal variability plots clearly show that the UV continuum and emission-line intensities in the NE jet have been increasing at a constant rate over the period of *IUE* observations 1982–1989. This provides evidence that the source is directing its highly collimated flow at a constant rate, which would be indicative of outflow from an accretion disk. An alternative model is proposed by Paresce & Hack (1994) in which two winds are colliding, one from the Mira and the other from the hot secondary, to form the highly collimated jet. We believe this scenario would be unable to produce such a well-collimated flow in this widely separated system which contains 386 day pulsating Mira because the collision of two inherently unstable winds from the Mira and hot secondary would produce an even more unstable combined wind. Finally, the fact that the NE jet is increasing, while the SW counterjet is decreasing in intensity, argues for a precessing mechanism associated with this system. If a bipolar wind emanating from the accretion disk collides with the stationary condensations of matter, it could produce emission lines through collisional ionization and recombination as the gas cools. Therefore, we believe a precessing disk with a changing direction of collimated flow could be responsible for the increased activity in the NE jet.

The ultraviolet spectra of the H II region in Figures 2*a*–2*d* clearly display a UV continuum flux distribution and emission-line intensities which have increased by factors of ~2–3 over the period of *IUE* observations (1979–1992). Moreover, the temporal variability plots (Figs. 5*a*–5*h*) provide further evidence that the total integrated UV flux and emission line intensities are increasing. The detection of N v, which has steadily increased since 1986 October, also suggests a region of high excitation, perhaps a postshock high-temperature region. Evidence for shock speeds up to several hundred km s^{-1} has been presented by Solf (1992) and Michalitsianos, Perez, & Kafatos (1994). However, as mentioned above, there is no evidence from the overall *IUE* line intensities requiring shock temperatures of $\geq 10^5$ K as one would expect for a shock with $V_s \geq 300$ km s^{-1}. Since the *IUE* 10″ × 20″ aperture encompasses the H II region and feature A (Michalitsianos & Kafatos 1988), and previous observations of features A and B exhibit N v and He II, we believe that feature A is responsible for the increase in the emission-line intensities and the presence of N v λλ1238, 1242 and He II λ1640 in the H II region spectra. The results in Table 4 show that the size of the H II region line-emitting region is increasing while the electron density is declining, confirming that the emitting volume is becoming larger. This is in agreement with Solf (1992), who found the H II region to be expanding at a rate of 40 km s^{-1}. An expanding emitting volume and declining electron density may indicate an expansion of material that was previously shock heated.

Alternatively, photoionization of circumstellar material by a hot ionizing source may account for the increased line intensities and continuum flux in the jet. However, a minimum ionization temperature of ~80,000 K would be needed to provide the necessary N v excitation, a temperature that may be unreasonably high for this system. In other words, the overall ionization state obtained by *IUE* does not provide evidence for such high states of ionization. If photoionization from an accretion disk is the dominant excitation mechanism, one may expect to observe X-ray emission from the inner regions of the accretion disk as material spirals into the hot subdwarf. Observations by Viotti et al. (1987) found only soft X-ray emission from the NE jet, although recent *ROSAT* observations (Kafatos et al. 1995) may indicate a soft X-ray point source.

In summary, the ultraviolet spectra obtained during 1979–1992 of the symbiotic star R Aqr confirm that features A, B, and D of the NE jet are increasing in intensity, consistent with the earlier predictions of Michalitsianos et al. (1986) and Kafatos et al. (1986). The increase in emission-line intensities may be due to an expanding emitting volume or a region which is increasing in excitation. We believe that shock excitation by a radiative shock may be a likely emission mechanism in the jet. It is possible that the lower ionization gas is photoionized (see Kafatos et al. 1986), perhaps by an accretion disk, while the high ionization material is shocked. The shock may originate as a bipolar wind emanating from an accretion disk which collides with the stationary clumps of matter (Solf 1992). The increase in emission-line intensities in the NE jet around 1983 may be a result of a precessing accretion disk (Michalitsianos et al. 1988) which is directing its collimated flow toward features A, B, and D. In the present analysis, a

combination of these two models would best explain the ultraviolet observations. We believe a highly collimated bipolar wind is produced by a precessing accretion disk. As the wind interacts with stationary condensations of matter (features A, B, D, and A′), a radiative shock is generated. A bipolar wind naturally accounts for the presence of the NE jet and the SW counterjet. Furthermore, a precessing accretion disk may be responsible for the increase in the UV continuum flux distribution and individual emission-line intensities in the NE jet and decrease in the SW jet if the bipolar wind is highly directional and collimated (Solf 1992).

Further observations of R Aqr with *HST* and *IUE* over extended periods along with contemporaneous coverage at X-ray and optical wavelengths would be helpful in understanding the complex physical processes of this star.

S. R. M. would like to thank A. G. Michalitsianos for many useful discussions and valuable comments concerning the manuscript. We would also like to acknowledge J. Mattei of the AAVSO for providing us with visual data on R Aqr. Finally, we thank Amy Martz, Cathy Imhoff, and Lyla Taylor of CSC and the staff of the *IUE* Image Processing Center for their assistance with all our reprocessing requests.

REFERENCES

Allen, C. W. 1976, Astrophysical Quantities (London: Athlone)
Anandarao, B. G., & Pottasch, S. R. 1986, A&A, 162, 167
Bath, G. T., Evans, W. D., Papaloizou, J., & Pringle, J. E. 1974, MNRAS, 169, 447
Brugel, E. W., Cardelli, J. A., Szkody, P., & Wallerstein, G. 1984, PASP, 98, 78
Burgarella, D., & Paresce, F. 1992, ApJ, 389, L29
Burgarella, D., Vogel, M., & Paresce, F. 1992, A&A, 262, 83
Hayes, M. A., & Nussbaumer, H. 1984, A&A, 134, 193
Herbig, G. 1980, IAU Circ., No. 3535
Hollis, J. M., Michalitsianos, A. G., Kafatos, M., Wright, M., & Welch, W. J. 1986, ApJ, 309, L53
Hollis, J. M., Oliversen, R. J., Kafatos, M., Michalitsianos, A. G., & Wagner, R. M. 1991, ApJ, 377, 227
Hummer, D. G., & Mihalas, D. 1970, MNRAS, 147, 339
Johnson, H. M. 1980, ApJ, 237, 840
———. 1982, ApJ, 253, 224
Kafatos, M., Hollis, J. M., & Michalitsianos, A. G. 1983, ApJ, 267, L103
Kafatos, M., Hollis, J. M., Yusef-Zadeh, F., Michalitsianos, A. G., & Elitzur, M. 1989, ApJ, 346, 991
Kafatos, M., & Michalitsianos, A. G. 1982, Nature, 298, 540
Kafatos, M., Michalitsianos, A. G., & Feibelman, W. A. 1982, ApJ, 257, 204
Kafatos, M., Michalitsianos, A. G., & Hollis, J. M. 1986, ApJS, 62, 853
Kafatos, M., et al. 1995, in preparation
Kaler, J. B. 1981, ApJ, 245, 568
Lepine, J. R. D., Le Squeren, A. M., & Scalise, E. 1978, ApJ, 225, 869
Lynden-Bell, D., & Pringle, J. E. 1974, MNRAS, 168, 603
Mattei, J. A., & Allen, J. 1979, JRASC, 73, 173
Mauron, N., Nieto, J. L., Picat, J. P., Lelievre, G., & Sol, H. 1985, A&A, 142, L13
Meier, S. R., Kafatos, M., Fahey, R. P., & Michalitsianos, A. G. 1994, ApJS, 94, 183
Michalitsianos, A. G., Hollis, J. M., & Kafatos, M. 1986, Canadian J. Phys., 64, 523
Michalitsianos, A. G., & Kafatos, M. 1982, ApJ, 262, L47
———. 1988, in The Symbiotic Phenomenon, ed. J. Mikolajewska et al. (Dordrecht: Kluwer), 235
Michalitsianos, A. G., Kafatos, M., & Hobbs, R. W. 1980, ApJ, 237, 506
Michalitsianos, A. G., Kafatos, M., Hobbs, R. W., & Maran, S. P. 1980, Nature, 284, 148
Michalitsianos, A. G., Oliversen, R. J., Hollis, J. M., Kafatos, M., Crull, H. E., & Miller, R. J. 1988, AJ, 95, 178
Michalitsianos, A. G., Perez, M., & Kafatos, M. 1994, ApJ, 423, 441
Murset, U., Nussbaumer, H., Schmid, H. M., & Vogel, M. 1991, A&A, 248, 458
Nussbaumer, H. 1986, A&A, 155, 205
Nussbaumer, H., & Storey, P. J. 1981, A&A, 99, 177
Osterbrock, D. E. 1974, Astrophysics of Gaseous Nebulae (San Francisco: Freeman)
Paresce, F., Burrows, C., & Horne, K. 1988, ApJ, 329, 318
Paresce, F., et al. 1991, ApJ, 369, L67
Paresce, F., & Hack, W. 1994, A&A, 287, 154
Pottasch, S. R. 1984, Planetary Nebulae (Dordrecht: Reidel)
Solf, J. 1992, A&A, 257, 228
Sopka, R. J., Herbig, G., Kafatos, M., & Michalitsianos, A. G. 1982, ApJ, 258, L32
Spitzer, L. 1978, Physical Processes in the Interstellar Medium (New York: Wiley)
Tylenda, R. 1977, Acta Astron., 27, 235
Viotti, R., Piro, L., Friedjung, M., & Cassatella, A. 1987, ApJ, 319, L7
Wallerstein, G. 1986, PASP, 98, 118
Wallerstein, G., & Greenstein, J. L. 1980, PASP, 92, 275
Whitelock, P. A. 1987, PASP, 99, 573
Whitelock, P. A., Feast, M. W., Catchpole, R. M., Carter, B. S., & Roberts, G. 1983, MNRAS, 203, 351
Willson, L. A., Garnavich, P., & Mattei, J. A. 1981, Inf. Bull. Var. Stars, No. 1961